Nano Energy 100 (2022) 107488

Contents lists available at ScienceDirect

Nano Energy

journal homepage: www.elsevier.com/locate/nanoen

Defected meta-lattice structures for the enhanced localized vibrational energy harvesting

Ali Hosseinkhani, Fariba Ebrahimian, Davood Younesian *, Armin Moayedizadeh

School of Railway Engineering, Iran University of Science and Technology, Farjam St, Tehran 16846-13114, the Islamic Republic of Iran

ARTICLE INFO

Keywords:
Auxetic
Phononic
Defect
Energy harvesting
Piezoelectric

ABSTRACT

This study focuses on the application of the meta-lattice structures for the energy conversion enhancement in piezoelectric energy harvesters. Three auxetic patterns are designed aiming at efficient energy conversion and a novel phononic crystal is suggested for the mechanical wave manipulation. Based on the supercell calculations, the bandgap features are extracted on the Irreducible Brillouin Zone. The auxetic patterns are embedded in the perfect crystal to act as a functionalized defect, disturb the periodicity of the perfect crystal, and create several bandpasses over the main bandgaps. The defected supercell is located inside a two-dimensional metaplate to investigate its performance in vibration energy harvesting. Numerical modeling of the metaplate is provided in order to show the energy concentration on the defect location and energy harvesting enhancement. The numerical model is validated by experimental tests. It is found that the Auxetic patterns remarkably enhance the performance of the energy harvesting system between 1.29 and 5.26 times in different designs.

1. Introduction

Energy Harvesting (EH) converts background ambient energy to the useful electricity in order to power low-consumption, self-powered electrical devices [1–3]. This closed-loop energy generation/consumption has several applications in nano-devices, sensor networks, health monitoring, smart transportation systems, and IoT [4–6]. Energy harvesting is a logical approach to prevent battery replacement and wiring in remote/mobile electronic devices [7]and to provide electricity for thousands of distributed sensor nodes [8,9]. Among the different EH methodologies, Piezoelectric Energy Harvesting (PEH) is a popular and straightforward methodology that provides operational power for electronic devices [10]. PEH devices are usually operated by use of vibrational energy that is available and ubiquitous everywhere and the basic principle of each harvesting device is to harness the energy around the device and convert it to useful electrical power [11,12]. Nevertheless, the range of generated power may not be sufficient in several PEH cases because the surrounding vibrational energy is usually expanded on a vast area with low energy levels, and converting it to electricity is usually low-efficient [13]. This fact has propelled much attention toward the field of Energy Harvesting Enhancement [14,15]. Recently, the properties of metamaterials have opened their path to the field of energy harvesting to considerably increase the range of harvested power from an EH system [16–21].

Metamaterials are a new class of artificial materials with extraordinary properties which cannot be obtained in conventional materials [22–24]. Mechanical metamaterials also known as auxetics exhibit a negative Poisson's ratio, a behavior not observed in conventional materials [25,26]. Auxetics have a wide range of Poisson's ratios that make them practical for different functions and applications [27–29]. Integration of auxetic materials with strain-based energy harvesting has been introduced as a way to raise the power-to-mass ratio of the EH devices [30–32]. The conversion of strain energy into electricity in the PEH with auxetic substrates is more efficient due to the negative sign of Poisson's ratio [33]. Also, the cellular nature of an auxetic structure provides more strain and stress concentrations which cause more electrical output from a PEH device [34]. The addressed methodology has been used in different devices including a bimorph energy harvester [35], low-frequency acoustic energy harvesters [36], auxetic Nanogenerators [37], and Micro-Electro-Mechanical-Systems [18] to enhance the device performance.

Phononic crystals, another class of metamaterials, are well-known due to the feature of bandgap: a frequency range over which the propagation of elastic waves is stopped [38]. The bandgap feature donates the phononics the capability to manipulate elastic waves [39–42]. There are generally two methods for the creation of bandgaps. The first

* Corresponding author.
E-mail address: Younesian@iust.ac.ir (D. Younesian).

https://doi.org/10.1016/j.nanoen.2022.107488
Received 6 January 2022; Received in revised form 2 May 2022; Accepted 7 June 2022
Available online 11 June 2022

method uses the employment of an arrangement of local resonators which is named Locally Resonant Acoustic Metamaterials (LRAMs) [43,44]. The second method for the formation of bandgaps is originated from the changes in geometry or properties of a material. This method is known as Bragg's scattering method and it is due to refractions and diffractions of the elastic wave at discontinuities [45,46]. Geometrical variations in periodic and cellular materials are a common reason that usually leads to the realization of the bandgap. In this regard, the bandgap features are significantly influenced by the internal geometry of the lattice structure [47,48]. The resulting lattice structure is known as the "phononic crystal."These crystals are able to completely stop wave propagation [49], act as frequency filtering tools, and work as wave guidelines [50,51]. All of these capabilities are because of the addressed property of the "bandgap." The introduction of a defect or imperfection, however, disturbs the bandgap frequency features and creates several bandpasses through the bandgap. Over these frequency bandpasses, the elastic/acoustic waves are able to propagate and travel through the cellular crystal. Since the appeared bandpass frequencies are related to the mode of the defect, the defect resonates at these frequencies [52]. Therefore, the vibrational energy will be localized at the location of the defect on the frequency of bandpasses and the harvested energy from this focal position is drastically higher than harvested energy from conventional devices [53,54]. Through the employment of defected crystals, about 13–625 times power enhancement has been achieved in different researches [55–58].

The practical application of metamaterial-based energy harvesting from vibrational energy becomes more highlighted in high frequency ranges. The concept of vibration energy harvesting might be employed in different frequency ranges from infra-sound to ultra-sound vibrations [11,12]. Each vibrational harvesting device must be tuned at a practical resonance frequency on which the device has the best output power. In ultrasound range, the design of a resonating element with a resonance frequency of kHz leads to micro-scale resonators, and due to their size, they are not able to harness sufficient power for electrical devices. This means that conventional resonators which are suitable in the infra-sound regime are not applicable in ultra-sound vibrations. Therefore, they are replaced by energy localizers in the high-frequency range [12,53]. Another horizon for metamaterial-based energy harvesting can be addressed in multi-functional applications for designing a self-protected structure against unwanted vibrations/noise. Metamaterial energy harvesting can be introduced to ease the complex problem of integrated passive and active control methods along with health monitoring. Metamaterials by themselves are among the robust passive control methods with wide, tunable frequency characteristics by which a great portion of incoming waves can be trapped/guided away from sensitive locations of a structure [59]. At the same time, the trapped energy can be pumped into a harvesting device to provide the electrical energy required for sensors and actuators used in the active control and health monitoring systems [16,60]. Once the mechanical and electrical properties of a metamaterial are combined, the bandgap features become designable according to any practical application [61–63].

Mechanical waves available in the environment usually have a low energy level. Converting their energy to electricity by using piezoelectric materials has also low efficiency in general. These two challenges restrict the performance of energy harvesting systems and prevent them from supplying self-powered electronic devices. In case of the PZT energy harvesting from elastic waves in the plate structures this limitation becomes more challenging since the content of input energy is very low compared with the tuned resonators. In order to solve this challenge, researchers have already used solid defects to localize the energy in a latticed structure. This concept has worked in practice however increasing the value of extracted power is still in demand. As a novel concept, we are proposing an auxetic defect to remarkably enhance the value of extracted power. This new idea has no extra cost for material or size change. It is proved that by this new concept, a magnification factor

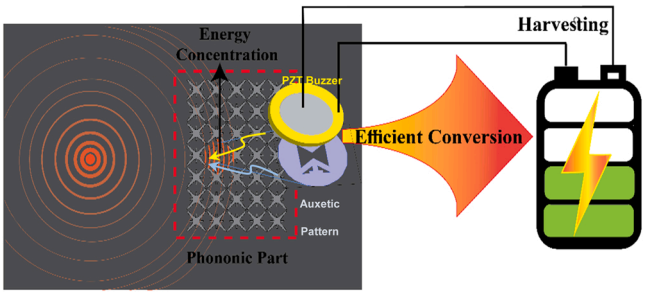

Fig. 1. The general process of metamaterial energy harvesting including: phononic crystal for energy concentration, auxetics for efficient energy conversion, and piezoelectric for harvesting electrical power.

of 5 and even larger can be achieved. It is shown that the idea can be practically applied to the PZT substrate by a simple laser cutter with reasonable fabrication cost. We experimentally prove the concept in a test set up. Sort of other geometrically singular non-auxetic defects are also taken into calculations. It is shown that auxeticity has dominant effect compared with the solid and singular defects. The general idea of this research is schematically illustrated in Fig. 1. Propagation of the mechanical wave is shown in a two dimensional plate while the phononic segment is able to manipulate mechanical waves and concentrate them into a focal point. An auxetic design and piezoelectric element are embedded in the focal point and the auxetic pattern helps the piezoelectric element to have higher conversion efficiency.

2. Concept and numerical modeling

2.1. Auxetic concept

Fig. 2(a)–(c) illustrates the schematic of three auxetic cells from the top view. The geometrical parameters of each cell are all defined over the schematics. Each one has a square shape design ($L_1 = L_2$) and they are named auxetic I, II, and III, respectively. The parameters used for the presentation of the auxetic structures are: t_i used for the rib thickness; L_i used for the length of auxetic cell;$c_i$used for the crossbeam length;$\alpha$and$\beta$and$\theta_i$used for the cell angles. The values which are considered for these parameters are listed in Table 3. The deformation contours of auxetic designs in a simple tension test (x direction) are shown in Fig. 2(d)–(f). Influences of negative Poisson's ratio cause the cells to expand in both directions, simultaneously. Also, if these designs undergo a compression load, they shrink in both x and y directions. This behavior stands against what happens in conventional materials that is aimed to be used in energy harvesting enhancement.

Auxetic I is well-known and among the first suggested auxetics used in the literature of energy harvesting [15]. Star-shaped auxetics (unit cell III) are also investigated in the history of the metamaterials [64] which are an expansion of the auxetic I. In both of them, the main technique that causes negative Poisson's ratio is inward ligaments. This technique is combined with a circular-shaped auxetic pattern to construct the architecture of auxetic II. This pattern is geometrically matched with the circular shape of the PZT buzzer [34]. Therefore, auxetic II has a circular shape from the internal view and a polygon shape from the external view. As seen in Fig. 2(e), the sharp edges have the highest auxeticity feature in the auxetic II and they will induce extra stress/strain concentration.

The auxetic structures actually increase the power-to-weight ratio of piezoelectric harvesters according to two principles: the first one is associated with the well-known equation that presents the relationship between average of stresses and output power in piezoelectric materials [15]:

$$\text{power} \propto (\sigma_{11} + \sigma_{22})^2 \quad (1)$$

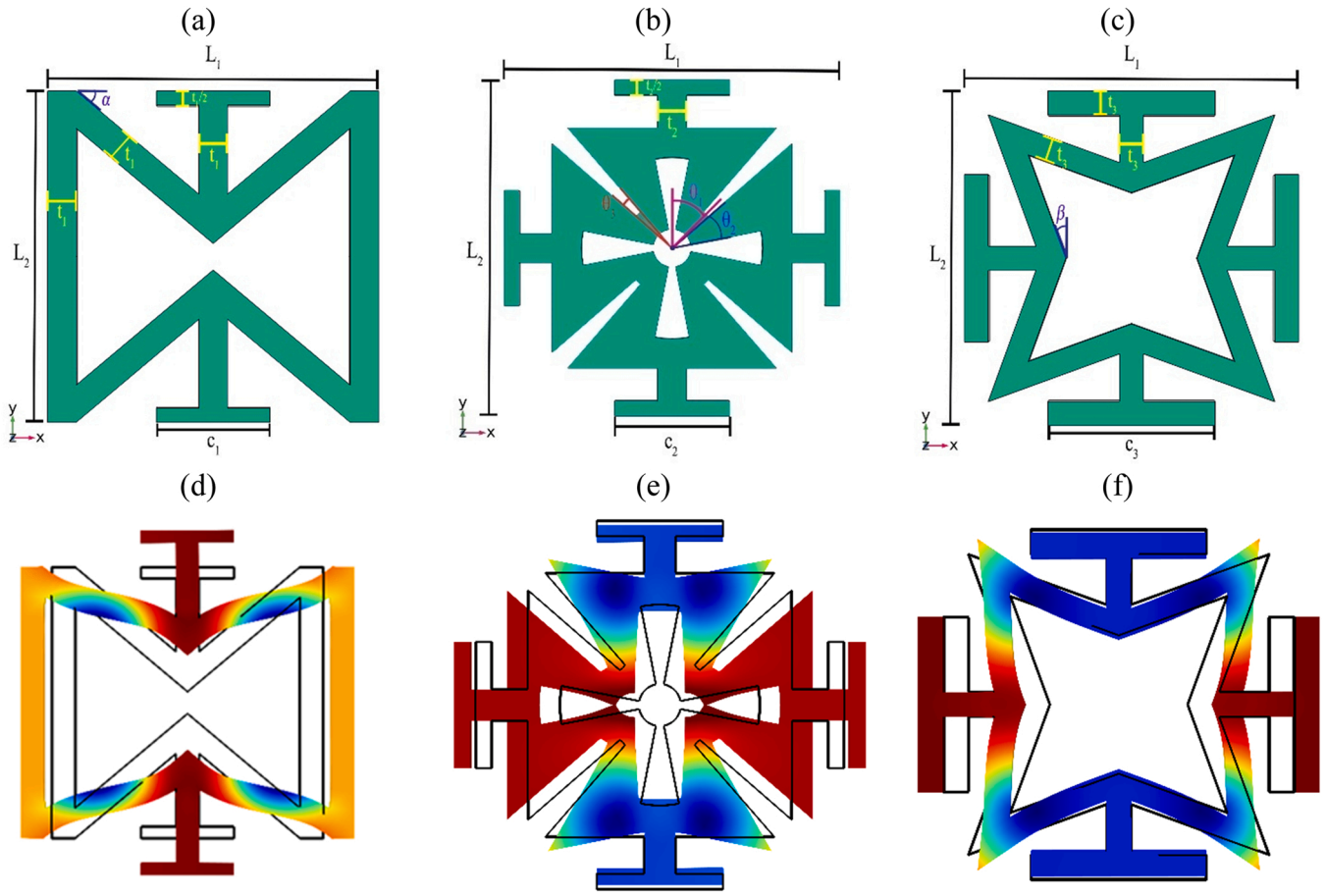

Fig. 2. Schematics of auxetic desings and their geometrical parameters: a) auxetic I, b) auxetic II, c) auxetic III. Deformation and auxetic behavior of the designed cells: d) auxetic I, e) auxetic II, f) auxetic III.

where σ_{11} and σ_{22} represent the average stresses in the main directions. In conventional materials, due to the positive sign of Poisson's ratio, these stresses have opposite signs. In the auxetic materials, however, the main stresses have the same sign that leads to significant enhancement of the generated power from a piezoelectric transducer.

The cellular nature of the auxetics creates singular geometrical regions and corners that is the second principle that increases the power-to-weight ratio of piezoelectric harvesters. The stress concentration in these points is much higher than in a uniform structure. Therefore, more stress concentration and more harvested energy from a piezoelectric material can be achieved according to the following constitutive equations [65]:

$$S_1 = s_{11}^E T_1 + d_{31} E_3$$

$$D_3 = d_{31} T_1 + \varepsilon_{33}^T E_3 \quad (2)$$

where S_1 is strain in the longitudinal direction, T_1 is stress in the longitudinal direction, s_{11}^E is electric compliance of a constant electric field, d_{31} is piezoelectric strain, D_3 is charge density, E_3 is electric field, ε_{33}^T is dielectric constant under constant stress. Therefore, according to the two addressed principles, an auxetic pattern is able to several times enhance the conversion of mechanical energy into electrical energy.

2.2. Bandgap and bandpass analysis

The phononic crystal that is used for the manipulation of vibrational waves is built from the two-dimensional arrangement of a novel unit cell. Schematic of one unit cell and the occasioned supercell are respectively shown in Fig. 3 (f) to (h) from the top view (x-y plane). The unit cell main parameters are defined at this figure. A great number of unit cells can be proposed and employed for the phononic concept. The proposed concept will work if this design is replaced by any other phononic structure however each configuration of the unit cell has its own dispersion properties.

The idea behind the design methodology of the present phononic unit cell originates from the sinusoidal form of a propagating elastic wave. The design steps are presented in Fig. 3(a)–(e) that are described as follows:

(I): A curve with a sine equation is created with negative offset value of W (Fig. 3(a)).

(II): Two lines parallel to the y-axes with length of W are drawn while a perpendicular straight line with the length of l completes one quarter of the unit cell. The internal area of the created lines is converted to a solid region (Fig. 3(b)).

(III): An Isosceles triangle as depicted in Fig. 3(c) is plotted while its head is concentric with the center of the phononic unit cell. The length of the triangle edges is a and b.

(IV): the area surrounded by the triangle is removed from the previous curved shape solid area and the region depicted in Fig. 3(d) is achieved.

(V): in the last step, by use of mirror and copy commands in the software the achieved quarter is developed to the unit cell and by use of the union command, the phononic unit cell is finalized (Fig. 3(e)).

In overall, we have four parameters (A, a, b, w) by which the design of unit cell is obtained while the unit cell length is fixed to l = 3 cm. These four parameters also can be used for tuning the bandgap features. Calling a first wide frequency bandgap, an optimization problem is

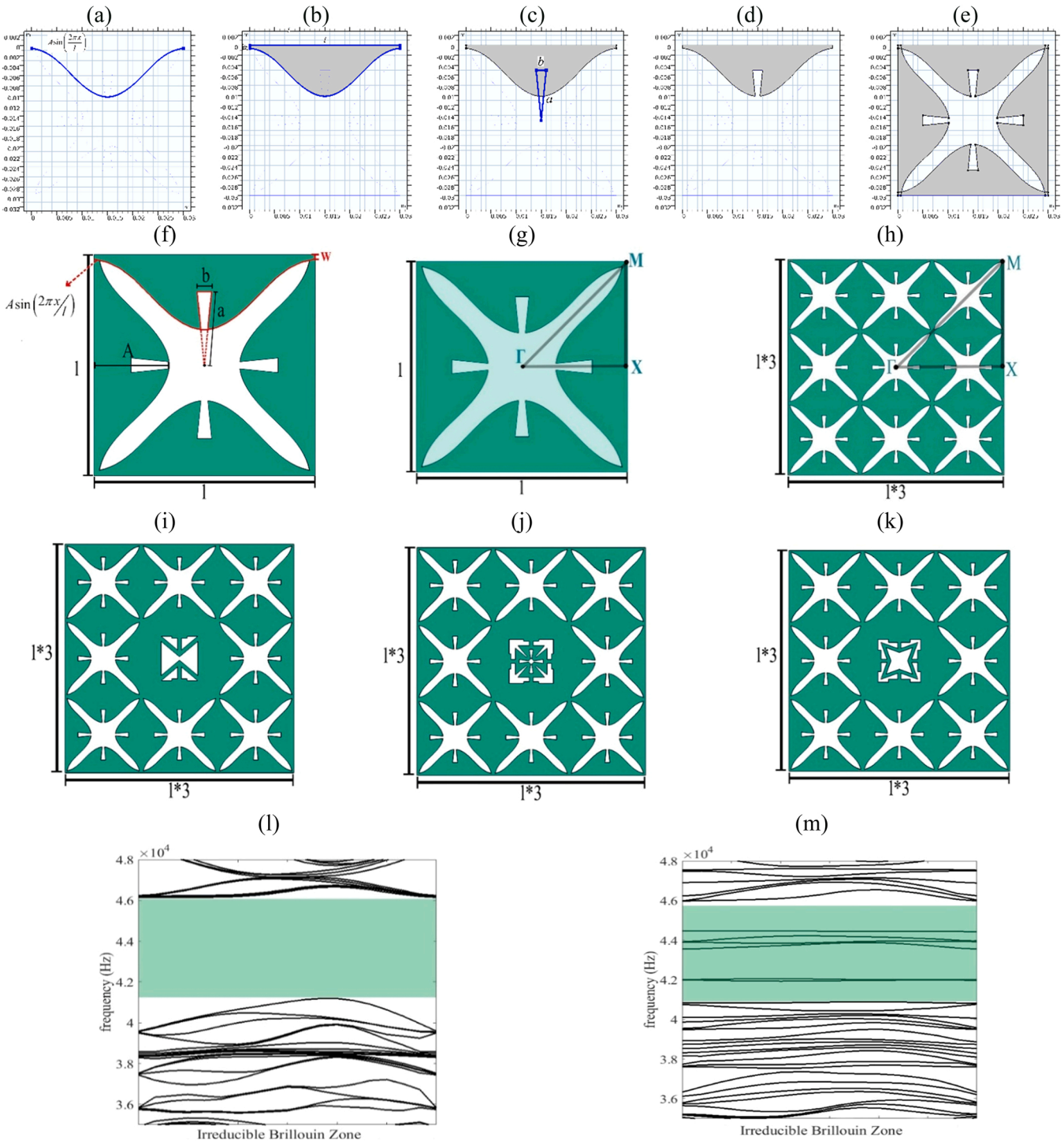

Fig. 3. Schematics of (a-e) design steps of phononic,(f) finalized unit cell and its geometrical parameters (g) unit cell and IBZ (h) perfect 3 * 3 super cell. The defected supercells with (i) auxetic design I, (j) auxetic design II, (k) auxetic design III. Bandgap diagram of (l) perfect supercell and (m) defected super cell.

Table 1
Optimized parameters of phononic unit cell.

Parameter	A	w	a	b
Value (mm)	4.8	0.4	10	2

constructed as presented in Eq. (3).

$$\begin{aligned} &\text{Objectivefunction}: \text{FBGW}(A, w, a, b) \\ &\text{Parametersrange}: \\ &3\text{mm} < A < 5\text{mm}; 0.2\text{mm} < w < 2.2\text{mm}; 6\text{mm} < a < 12\text{mm}; 1\text{mm} < b < 10 \\ &\text{constrain}: \text{BGW} > 1000\text{Hz} \end{aligned} \tag{3}$$

The problem is solved by use of the Genetic Algorithm. The optimized geometrical parameters of the unit cell are presented in Table (1).

The optimization is conducted to make sure that there is a wide

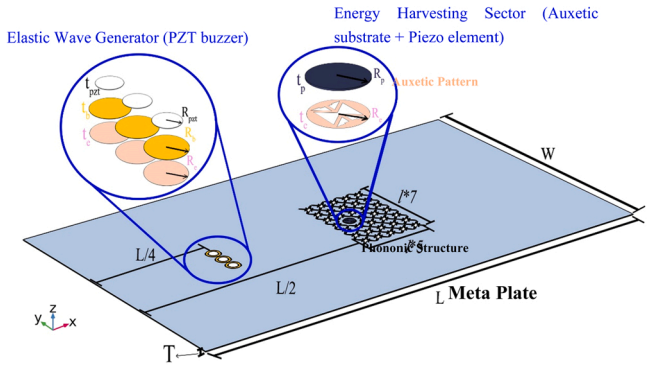

Fig. 4. Detailed view of the meta-plate numerical modeling.

bandgap on which the bandpasses occur. After defining the defect, and moreover, due to fabrication errors, it is possible that the width of bandgap frequency changes to some degrees. Therefore, having a wider bandgap ensures bandgap and bandpasses are still working during the experimental test.

Bandgap calculations for a unit cell are based on the theory of Bloch that investigates wave propagation over one unit cell of a periodic structure. After calculating bandgap features for one unit cell, the features are repeated and replaced in x- and y-directions of the crystal with the periodicity of lattice constant. Supercell calculations can be achieved from bandgap analysis of the unit cell and from the band folding method [66]. Therefore, the supercell calculation is used to investigate the phenomenon of waveguiding and wave localizing in defected crystals [67,68].

In order to concentrate the energy of an incident vibrational wave, a single defect is proposed in the present research. The defect must have different geometry or material properties compared to the perfect structure, and this imperfection creates several defect modes in the bandgap diagram of the perfect structure. Here, the structure of the defect follows a cellular auxetic pattern which is a new idea to increase to energy conversion efficiency. Three auxetic designs introduced in Fig. 2 are used in the construction of three defected crystals. Schematic of defected supercells with different auxetic designs are depicted in Fig. 3(i)-(k).

The inclusion of a defect creates several bandpass frequencies which are related to the resonance of the defect. The bandgap diagrams are calculated from Bloch's theory and they are plotted for a perfect supercell and for a defected one in Fig. 3(l) and (m), respectively. The commercial software COMSOL Multiphysics is used for the calculation of the bandgap diagrams. As we can observe, there is a full bandgap over the frequency range of 41.2–45.5 kHz for the perfect structure (Fig. 3 **(l)**). The emergence of several bandpasses on the bandgap is seen in Fig. 3 (m) related to the defect modes. On these bandpasses, the vibrational wave passes through the cellular segment, and its energy is concentrated on the defect location because the defect goes into resonance condition. The material used for the simulation of supercells is aluminum and its mechanical properties are listed in Table 5.

2.3. Meta-plate simulation

This section explains the numerical simulation related to the meta-plate including phononic segment, auxetic defect, and also piezoelectric disks used as input exciter and output receiver. A detailed view of the meta-plate modeling is presented schematically in Fig. 4. The meta-plate is a rectangular plate and its width, length, and thickness are presented with W, L, and T, respectively. The clamped boundary condition is applied to the start and end edges in the x-direction and the edges are free in the y-direction. The middle point of the plate is the starting location of the phononic segment while it is continued into x-direction by a 5*l length. The phononic segment is extended into up and down y-direction with the length of 3.5*l which makes the total length of the phononic segment in y-direction equal to 7*l. The location of the defect is selected in the second column and middle row (as shown in Fig. 4).

Auxetic designs are considered as the defect structure and they act as the substrate of the piezoelectric energy harvester. Therefore, the piezoelectric harvester (1 mm Barium Titanate) is bonded on the auxetic substrate and at the middle of the defect location. The output voltage is received from the piezoelectric harvester. Three piezoelectric disks (PZT 5 H) are glued to the plate in order to excite the structure at any specific frequency. They are placed at a distance of 0.25 L from the left side of the plate and they can provide an input flexural semi-line wave. Geometry and location of piezo electrics and the epoxy used for bonding them to the plate are addressed in the figure. Also, the values for each parameter of Fig. 4 are presented in Table 3 and the material parameters are provided in Table 5. Material used for the construction of the meta-plate is aluminum with 1 mm thickness.

An input sinusoidal voltage with the amplitude of 26 Volt is applied to the terminals of piezoelectric actuators. The actuators excite the metaplate and a vibrational flexural wave propagates through the structure. The frequency of input signal sweeps around the bandpass frequencies to investigate the wave propagation on bandgaps and bandpasses. Each auxetic defect creates several bandpasses while for each design one bandpass is the strongest and has the highest ability for energy concentration. From the frequency sweep, the displacement diagram for the defected structure with auxetic designs is achieved. They are plotted against a plain structure, and by the plain structure, we mean a homogenous plate with the same size but with no cellular segment. We see that on the resonance frequencies, the displacement of meta-plates is far larger than the displacement of the plain structure.

Surface displacement contours for the meta-plates at the resonance frequency are illustrated in Fig. 5(a)–(c), while auxetic designs of I, II, and III are used as the defects. The considered frequencies in Fig. 5 are the same as the resonance frequencies in Fig. 6 (a). It is seen that surface

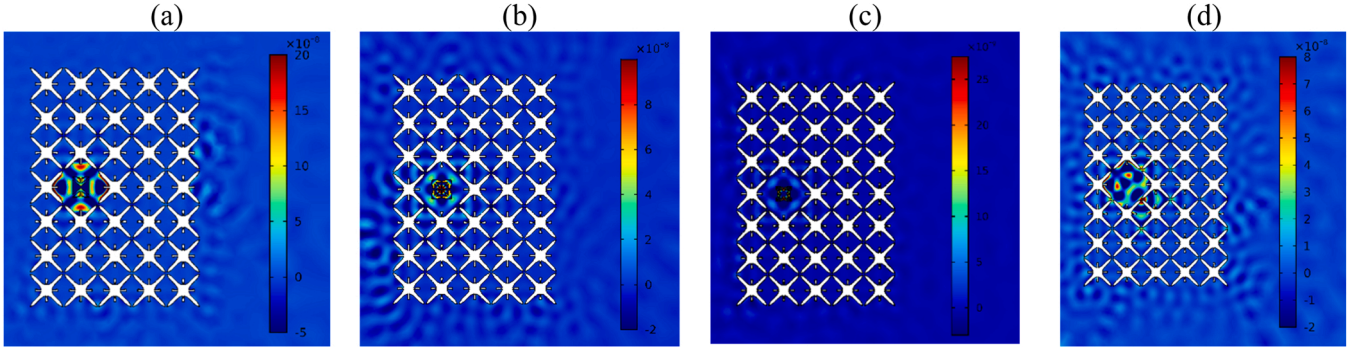

Fig. 5. Surface displacement at the resonance frequency of meta-plate for the defected crystals with (a) auxetic I (b) auxetic II and (c) auxetic III (d) non-auxetic (solid).

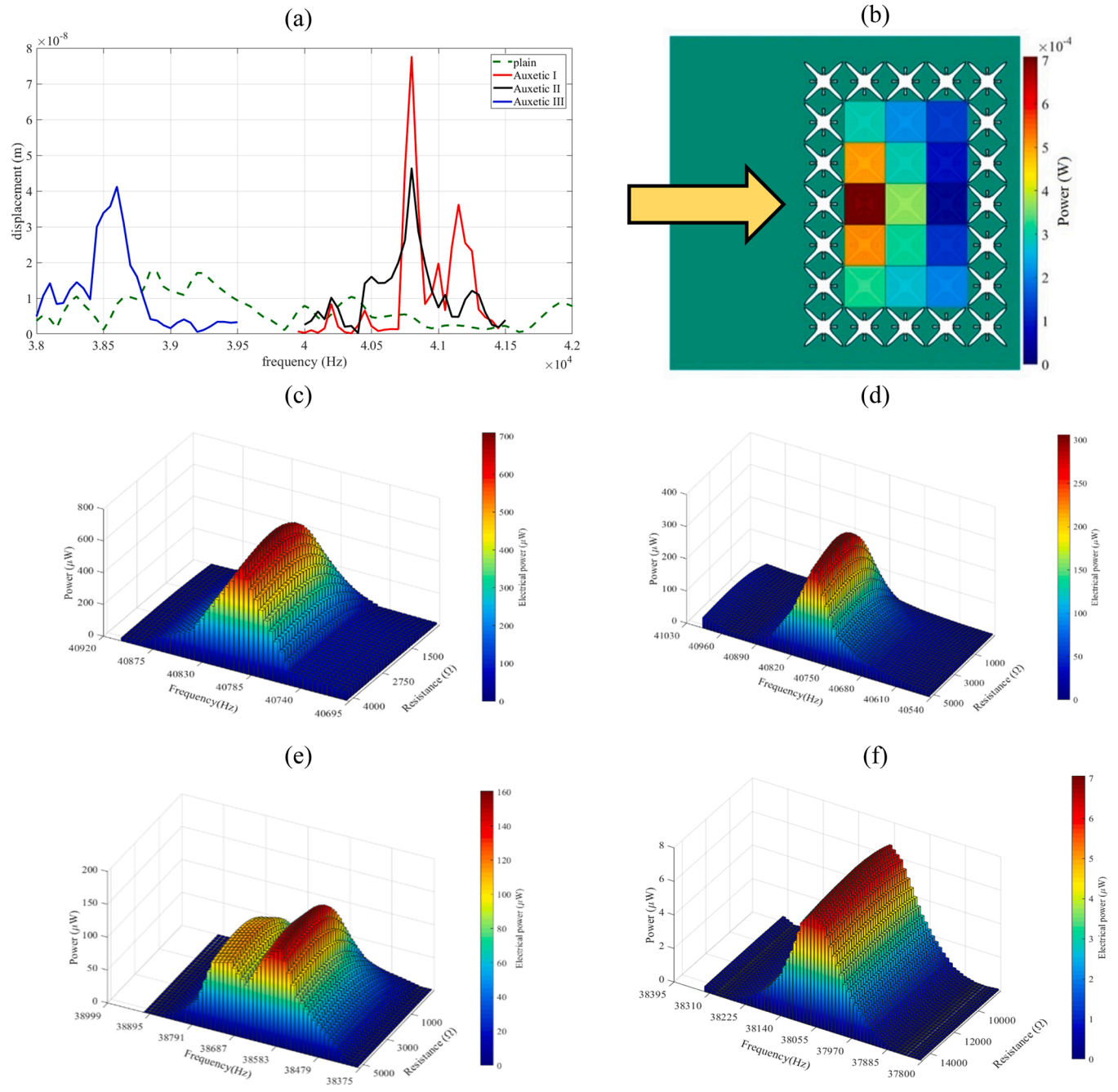

Fig. 6.. a) Displacement response of the metaplates with auxetic designs and the plain structure. (b) Electrical output power at different positions of defect within the phononic structure (auxetic I). Three dimensional diagram of power versus excitation frequency and electrical resistance for: (c) auxetic I, (d) auxetic II, (e) auxetic III and (f) plain structure.

displacement on the location of the defect is several times larger than displacement on the other areas. This shows that the vibrational energy is remarkably concentrated on the desire location.The displacement contour for the case of non-auxetic defect is also presented in Fig. 5. (d), which shows the concept of defected phonic for the energy concentration works for this case too. However, the level of energy concentration is much less than the other cases i.e. auxetic patterns.

Similar to any energy harvesting system that works efficiently on its resonance condition, the present energy harvester also has a resonance frequency on which the output power is maximum. Here, the resonance frequency is related to the defect structure.

Fig. 6 (c)–(f) shows three dimensional diagrams of the harvested power from the meta-plates while electrical resistance and excitation frequency are changing simultaneously. Electrical resistance is also an important parameter in the harvesting systems while using its optimum value significantly enhances the output power. From this figure, the optimum amount of power is achieved from tuning resonance frequency and finding the optimum electrical resistance. For the meta-plates with auxetic I: Power= 710 μWat 40,800 Hz and 2500 Ω, auxetic II: Power= 316 μW at 40,800 Hz and 3000Ω, auxetic III: Power= 160μWat 38,600 Hz and 3000Ω are achieved. For the Plain structure Power= 7.05 μW at 38,050 Hz and 12,000 Ω is obtained. The maximum amount of power enhancement ratio (amplification factor) is achieved for the metaplate with auxetic defect I and its value can be calculated to be 100.7. For the case of non-auxetic defected meta-structure whose surface contour is shown in Fig. 5(d), the maximum output energy is 135 μW at 40,800 Hz and 3000 Ω. If we divide the electrical power of auxetic defects by the power of the non-auxetic defect, we can reach to (160/

Table 2
Power density achieved form different enrge harvesting cases.

Case	Aux I	Aux II	Aux III	Non-aux	plain
Power (W)	710e-6	316e-6	160e-6	135e-6	7e-6
Power density (W/m^3)	1.446e+3	0.643e+3	0.326e+3	0.275e+3	0.014e+3

135) 1.185 magnification factor for the case of aux III against the non-auxetic defect and to (710/135) 5.259 magnification factor for the case of aux I against the non-auxetic defect.

(In Fig. 6(b) effects of defect position (auxetic I) within the meta-structure are illustrated. Defect is placed in different 15 positions and the output power is calculated and symbolized by a color. In the research published by Jo et al. [69], it was concluded that there is an optimum position for the placement of a defect within each harvesting system. Also, it has been observed, performance of the harvesting device is enhanced when the defect is laced closer to the first layer from the side of the incoming wave. Here, we can see that the highest output power is achieved from the center position in the second layer.

It is interesting to compare the output power achieved from the three auxetic designs. As discussed, the phononic crystal with a defect is able to localize energy in a specific frequency range. The auxetic concept, then, enhance the energy conversion through the piezoelectric element. Auxetic feature influences the output power due to two principles which are both related to stress and strain. These two features are the negative sign of Poisson's ratio and the energy concentration in sharp edges. These two principles together enhance the output power of the three auxetic designs. The final results show that Auxetic I has the highest power. Design of Auxetic I has fewer sharp edges and stress/strain concentration compared to the auxetic II, however, it has more intensive auxeticity. This means that.

$Stress\ Concentrtion_{Auxetic\ I} < Stress\ Concentrtion_{Auxetic\ II}$ but $\upsilon_{Auxetic\ I} < \upsilon_{Auxetic\ II}$.

Comparing Auxetic I and II, the first one has one factor i.e. less Poison's ratio and the second design has the other factor i.e. stress concentration as the two dominant boosting factors. All in all, boosting factor in design I is stronger than it in design II and therefore the out power is larger in the Auxetic I. As result of the combination of the two principles we have: Power of Aux I > Power of Aux II > Power of Aux III.

Power density values for all of the designs are presented in Table 2.

The power density is calculated from dividing electrical power by the volume of the piezo-harvester material which corresponds to the volume of a cylinder with the radius of 25 mm and height of 1 mm that is equal to 4.91e-7 m^3.

In Fig. 7, four non-auxetic cellular defects including (a) solid, (b) circulare, (c) plus-shape and (d) square defects are illustrated. These defects are simulated and investigated in order to examine the advantage of using auxetic defects against non-auxetic defects. For the case of cantilever resonators, It has already been proved that auxetic patterns are an appropriate candidate to remarkably enhance the output power of the piezoelectric harvesting devices [15,34]. The enhancement is due to two concepts, i.e., (i) energy concentration and (ii) same sign principal stresses, as already explained in Section 2.1. In Fig. 7(e), the output powers from these non-auxetic patterns are shown and compared with output power from the auxetic I. We can see that the powers from non-auxetic defects are almost in the same level however very much less than the power calculated for the auxetic defect. Auxetic pattern amplify the extracted power by factor of 5–5.26 against non-auxetic defects. This enhancement can be justified from the stress results listed in Tables 3 and 4. Here, it is seen that average stresses when an auxetic defect is employed, have the same sign while they have different signs for the non-auxetic defects. According to Eq. (1), in the case of the auxetic substrate, summations of the principal stresses magnify each other. Furthermore, due to squaring the summation of stresses in the power calculation $(\text{Power} \propto (\sigma_{11} + \sigma_{22})^2)$, the effect of the "same sign stresses" is boosting the energy by power of 2. The absolute value of the principal stresses in the case of auxetic defect are also larger than those in the non-auxetic defects. This fact also further enhances the value of extracted power Table 5.

Table 3
Values of average stresses in x and y directions on in the piezoelectric element.

Case	Aux I	Non-aux-solid	Non-aux-circular	Non-aux-plus	Non-aux-square
$\bar{\sigma}_{11}$ (MPa)	-0.0366	+0.0337	+0.0346	+0.0336	+0.0321
$\bar{\sigma}_{22}$(MPa)	-0.1316	-0.0132	-0.0765	-0.0385	-0.0379

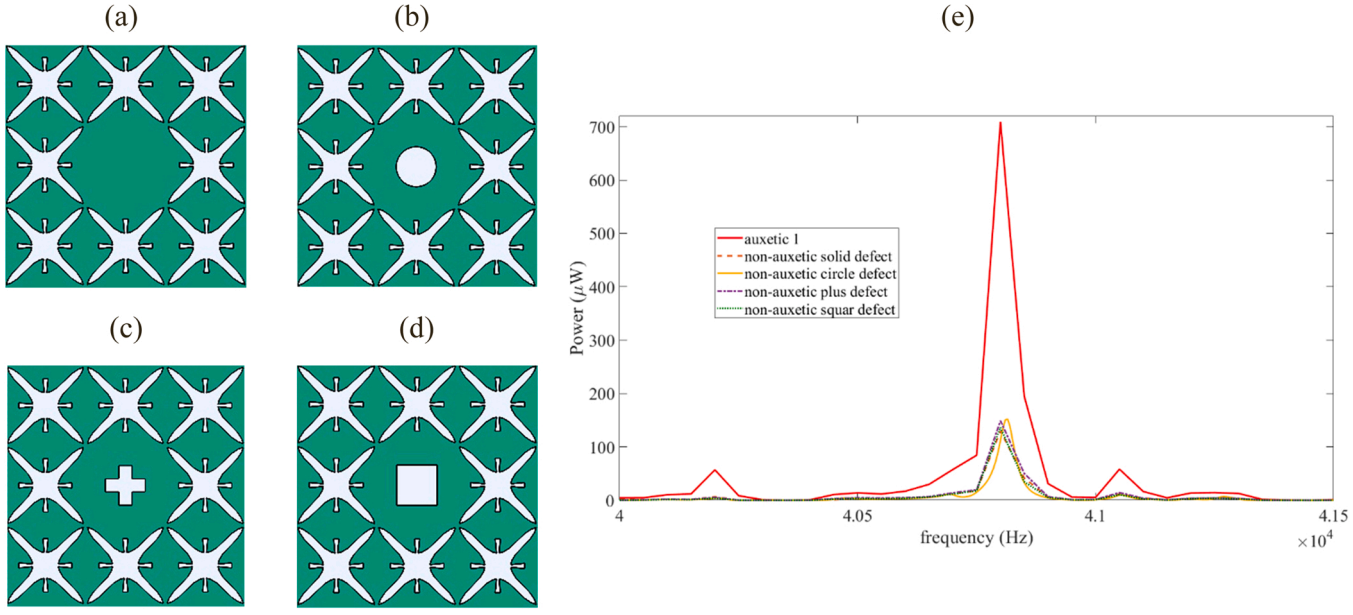

Fig. 7. Schematics of non-auxeitc (a) solid defect, (b) circular defect, (c) plus-shape defect and (d) square defect. (e) Comparison between the output power of auxetic I against power of different non-auxetic defects.

Table 4
Values of geometrical parameters used in the present research.

Part	Parameter	Symbol	Value	Unit
Piezo harvester	Radius	R_p	12.5	mm
	Thickness	t_p	1	mm
Epoxy element	Thickness	t_e	0.02	mm
	bonding strength	k	100	GN/m^3
Substrate element	Plate length	L	1000	mm
	Plate width	W	600	mm
	Plate thickness	T	1	mm
Piezo actuator	Radius	R_{pzt}	10	mm
	Thickness	t_{pzt}	0.02	mm
Brass of piezo actuator	Radius	R_b	15	mm
	Thickness	t_b	0.02	mm
Auxetic I	Length	L_1	17.5	mm
	Width	L_2	17.5	mm
	Thickness	t_1	1.5	mm
	Cell angle	α	40	deg
	Cross beam length	c_1	6	mm
Auxetic II	Length	L_1	17.5	mm
	Width	L_2	17.5	mm
	Thickness	t_2	1.5	mm
	Cell angle	θ_1	45	deg
		θ_2	30	deg
		θ_3	4	deg
	Cross beam length	c_2	6	mm
Auxetic III	Length	L_1	17.5	mm
	Width	L_2	17.5	mm
	Thickness	t_3	1.5	mm
	Cell angle	β	20	deg
	Cross beam length	c_3	7	mm

3. Experimental results

In order to compare numerical simulations with experimental results, three meta-plates as well as one plain structure are prepared and fabricated using a laser cutting method. In Fig. 7, the meta-plate samples used for the experimental test are presented beside the numerical models simulated in the software.

Fig. 8 illustrates the set up for the experimental test. A computer with the aid of a power source plays the role of the signal generator. Integration of the computer, power source, designed-board, and Arduino microcontroller 84 MHz provide a voltage signal with the amplitude of 26 Volt that is applied to the piezoelectric actuators. Pulse Width Modulation (PWM) code developed in the Arduino programming environment is connected to the board with the Arduino microcontroller. The input signal with the voltage of 26 V comes from the power source and after passing through the designed board, the desired frequency (between 38 and 45 kHz) is applied to the electrical signal. Therefore, a piezo-driver device is produced that is able to apply an electrical voltage with a certain amplitude and frequency to the piezo-actuators. The generated voltage is then delivered to piezoelectric actuators and a vibrational wave is created and it propagates to x and y-directions of the meta-plate. Both sides of the meta-plate are fixed in the longitudinal direction and are free in direction of width. One Barium Titanate piezoelectric harvester with a thickness of 1 mm is bonded on the defect location. The output voltage from the harvester element is read by use of an oscilloscope.

In order to convert output voltage into power, the electrical resistance is connected to the terminals of the piezoelectric harvester. The value of electrical resistance has a considerable influence on the harvested power and it has an optimum value for each energy harvesting system. In this regard, the electrical resistance is optimized for each case, and the power versus electrical resistance diagrams for the three meta-plates are presented in Fig. 10(a). Maximum power gained from meta-plates with auxetic I is 520 μW at the resonance frequency of 40579 Hz and the electrical resistance of 1300 Ω, auxetic II is 258 μW at the resonance frequency of 41916 Hz and the electrical resistance of 880 Ω, and for auxetic III is 150 μW at the resonance frequency of 39961 Hz and the electrical resistance of 6940 Ω.

Table 5
Mechanical properties for the materials used in the present research.

Material	Property	Symbol	Value	Unit
Brass	Density	ρ_b	8490	Kg/m^3
	Passion ratio	ν_b	0.31	
	Young modules	E_b	97e9	Pa
Epoxy	Density	ρ_e	1250	Kg/m^3
	Passion ratio	ν_e	0.35	
	Young modules	E_e	1e9	Pa
aluminum	Density	ρ_a	2700	Kg/m3
	Passion ratio	ν_a	0.33	
	Young modules	E_a	70e9	Pa
	Isotropic loss factor	η_a	0.0005	
Lead Zirconate Titanate (PZT-5H)	Density	ρ_{pzt}	7500	Kg/m^3
	Compliance matrix	S_{11}^E	1.65e-11	1/Pa
		S_{12}^E	-4.78e-12	1/Pa
		S_{13}^E	-8.45e-12	1/Pa
		S_{22}^E	1.65e-11	1/Pa
		S_{23}^E	-8.45e-12	1/Pa
		S_{33}^E	2.07e-11	1/Pa
		S_{44}^E	4.35e-11	1/Pa
		S_{55}^E	4.35e-11	1/Pa
		S_{66}^E	4.26e-11	1/Pa
	Coupling matrix		7.41e-10	C/N
		d_{15}	7.41e-10	C/N
		d_{24}	-2.74e-10	C/N
		d_{31}	-2.74e-10	C/N
		d_{32}	5.93e-10	C/N
		d_{33}		
	Relative permittivity	ε_{11}	3130	
		ε_{22}	3130	
		ε_{33}	3400	
Barium Titanate	Density	ρ_{bt}	6020	Kg/m3
	Compliance matrix	S_{11}^E	8.05e-12	1/Pa
		S_{12}^E	-2.35e-12	1/Pa
		S_{13}^E	-5.24e-12	1/Pa
		S_{22}^E	8.05e-12	1/Pa
		S_{23}^E	-5.24e-12	1/Pa
		S_{33}^E	1.57e-11	1/Pa
		S_{44}^E	1.84e-11	1/Pa
		S_{55}^E	1.84e-11	1/Pa
		S_{66}^E	8.84e-12	1/Pa
	Coupling matrix	d_{15}	3.92e-10	C/N
		d_{24}	3.92e-10	C/N

(continued on next page)

Table 5 (*continued*)

Material	Property	Symbol	Value	Unit
		d_{31}	-3.45e-11	C/N
		d_{32}	-3.45e-11	C/N
		d_{33}	8.56e-11	C/N
	Relative permittivity	ε_{11}	2920	
		ε_{22}	2920	
		ε_{33}	168	

Fig. 9 shows output power for the three meta-plates for auxetic I, II, and III. The calculated power from numerical simulation and experimental measurements are compared here. The measurements are implemented while the optimum electrical resistance is used for each case. It is observed that the maximum peak of frequency response is higher in numerical simulation that is due to ideal conditions that exist in the numerical modeling. Also, there are drifts(less than 3 %) between resonance frequencies which are mostly related to the boundary condition imperfections.

Energy Harvesting Enhancement is the main aim of the present research. As discussed, extraordinary features of two types of meta-materials are integrated here for the Energy Harvesting Enhancement. One feature is related to bandgap and bandpass properties of the defected metamaterials that concentrate energy at a specific location. The next feature comes from auxetic patterns while their NPR and cellular structure improve the conversion of mechanical energy to electrical power. The integration of energy concentration and efficient conversion significantly improves harvested energy from the presented meta-plates. The power amplification factor is presented in Fig. 10(b). This factor is calculated from the output power of each meta-plate divided by the power of the plain structure. For the plain structure, the output power of 6.73 μW is achieved from the experimental test and 7.05$\mu W$is achieved from numerical simulations. For the three meta-plates with auxetic defects, the power enhancement ratios achieved from numerical simulations are 100.7 (for auxetic I), 44.8 (for auxetic II), and 22.7 (for auxetic III). Also, the power enhancement ratios achieved from the experimental test are 77.3 (for auxetic I), 38.3 (for auxetic II), and 22.3 (for auxetic III) Fig. 11.

4. Conclusions

In the present study, two features of meta-lattice structures were combined for the piezoelectric energy harvesting enhancement. An auxetic defect on a photonic pattern were proposed as a new concept.

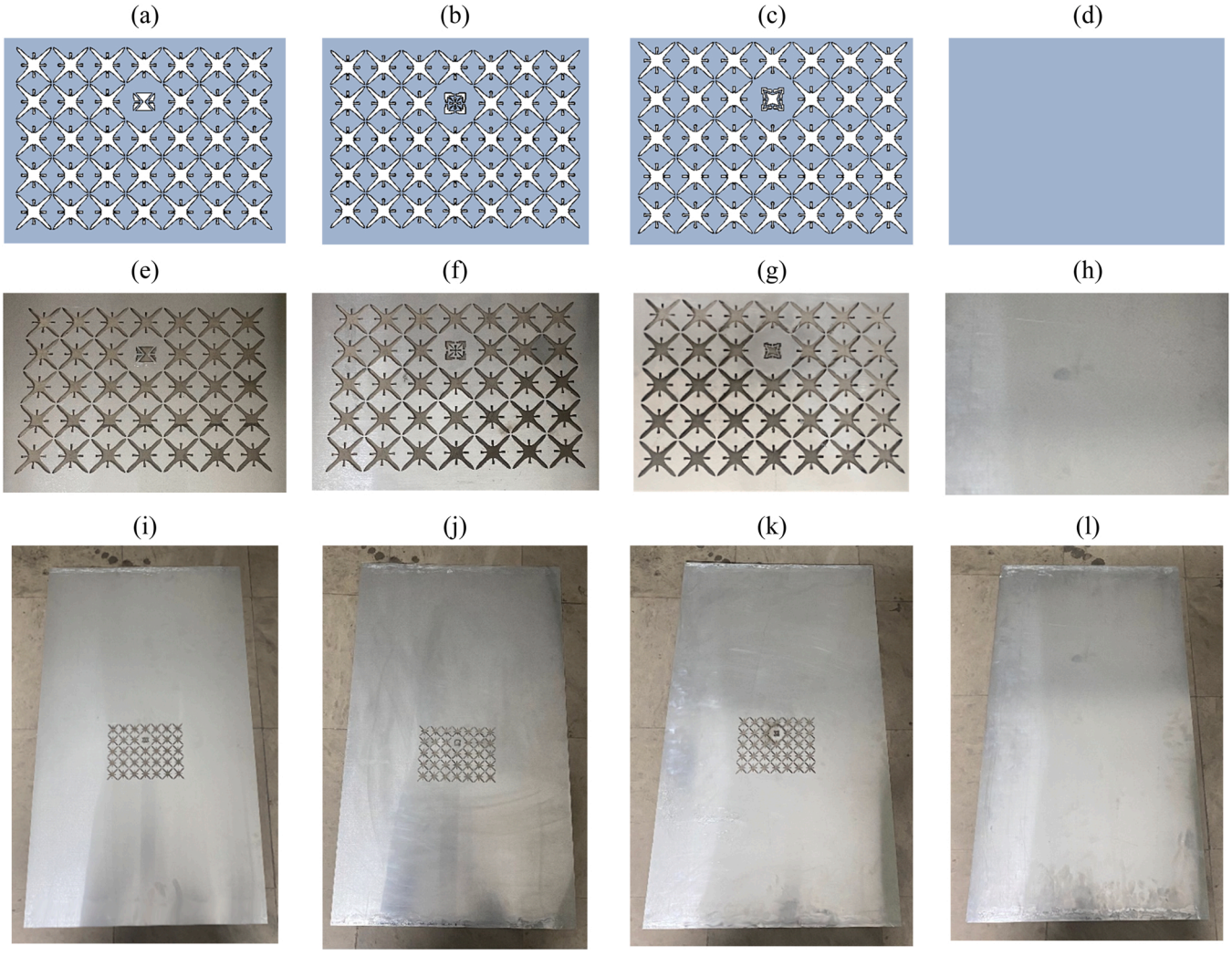

Fig. 8. Fabricated samples of the meta-plates for experimental test and simulation models; the cellular segment of numerical modeling for metaplates with (a) auxetic I, (b) auxetic II, (c) auxetic III; (d) the numerical model of plain structure; the cellular segment of fabricated metaplates with (e) auxetic I, (f) auxetic II, (g) auxetic III; (h)the fabricated model of plain structure; the complete illustration of fabricated metaplates with (i) auxetic I, (j) auxetic II, (k) auxetic III; (l) the complete illustration of the fabricated plain structure.

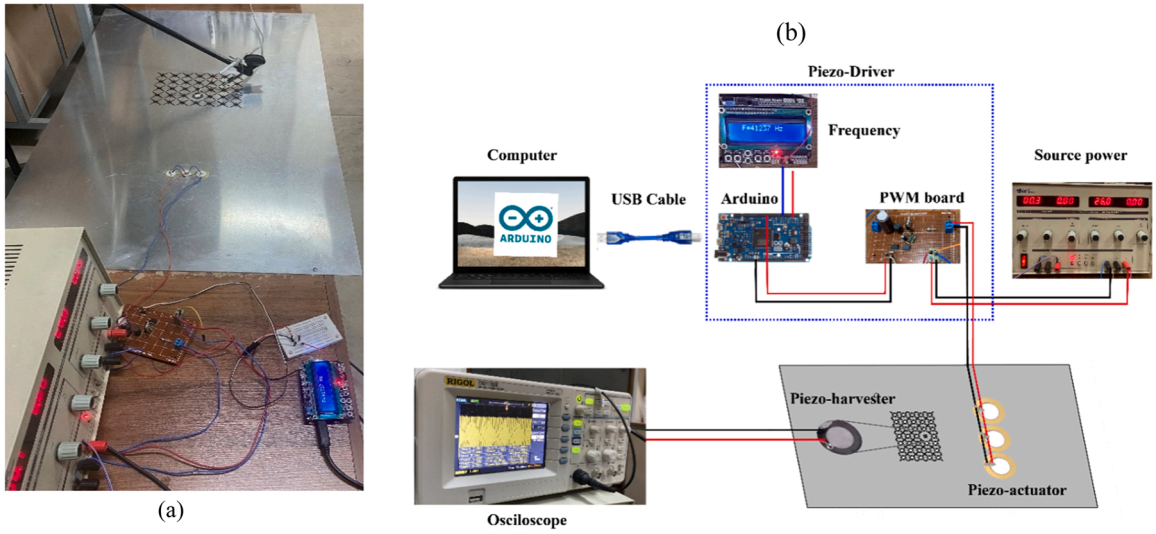

Fig. 9. (a) Experimental set up and (b) schematic of employed experimental equipment including Piezo-driver, metaplate structure, piezo-actuator, piezo-harvester, and oscilloscope.

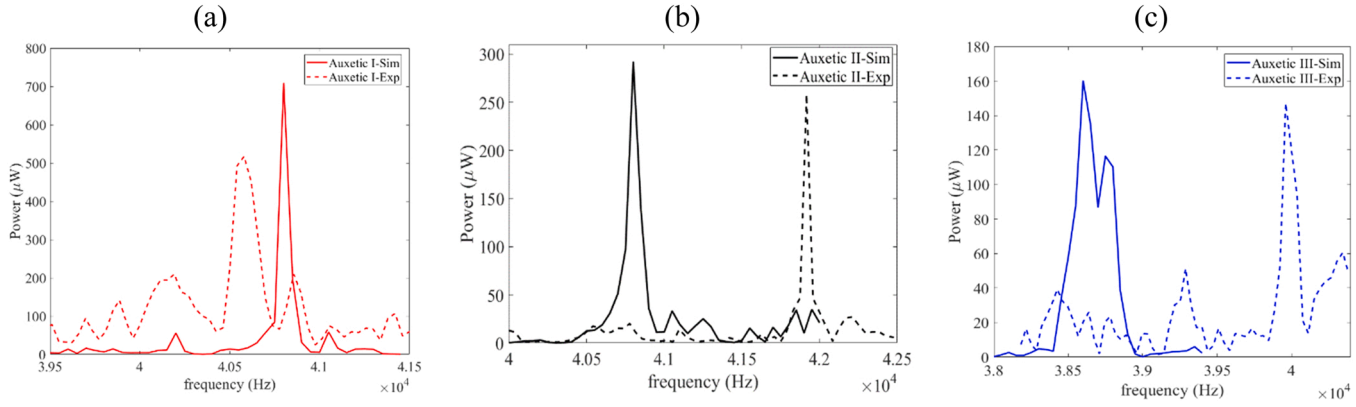

Fig. 10. Electrical power versus frequency from numerical simulation and experimental test for each metaplate at optimum electrical resistance.

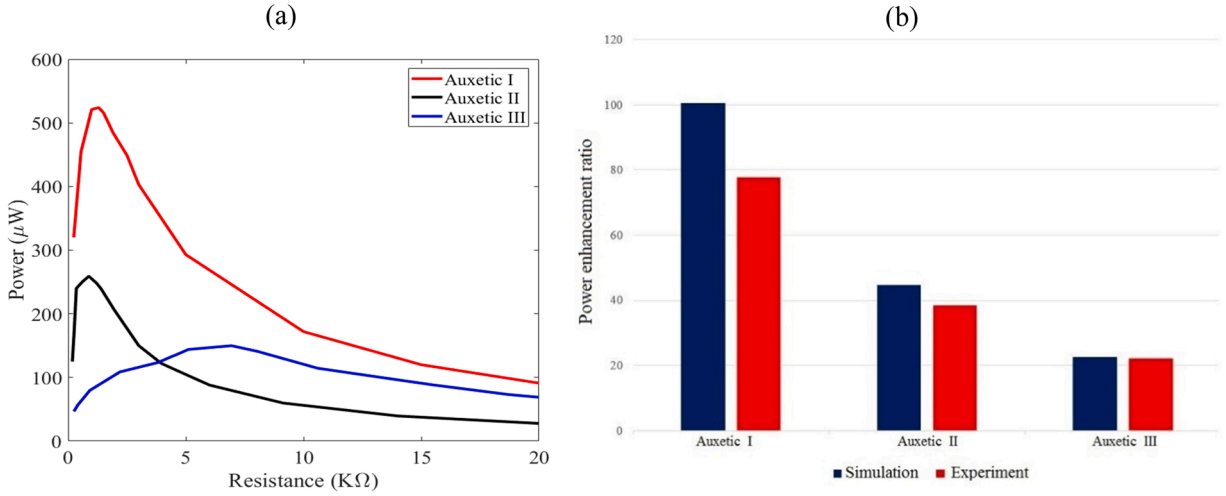

Fig. 11. (a) Experimental optimization of output power with respect to electrical resistance. (b) Power enhancement ratio of the three meta-plates from numerical simulations and experimental tests.

For this aim, novel defected phononic crystals were designed to concentrate energy and auxetic patterns were used for extra improvement in the conversion efficiency. Auxetic patterns were used as the defect on the perfect phononic crystal. It was observed that energy is precisely concentrated on the defect location. Displacement contours showed that the amplitude of dynamic response on the location of concentrated energy for the meta-plates is several times larger than a conventional structure response. Numerical modeling of the meta-plates

was implemented next to investigate energy harvesting enhancement via the addressed mechanisms. The meta-plates included the defected phononic segment, three piezo-actuators, and one piezo-harvester. The piezo-actuators excited meta-plate at any targeted frequency and the piezo-harvester converted the energy of mechanical waves to electrical power. By use of frequency tuning and electrical resistance optimization, the maximum output power was achieved from the numerical simulation and experimental tests. An experimental set up was developed here to verify the numerical simulations. The experimental samples of meta-plates were fabricated by laser cutting method and by use of a designed piezo-driver and piezo-actuators, the metaplates were excited at targeted frequencies. Well matching was observed between numerical and experimental results. The maximum energy harvesting amplification factor was achieved from defected crystal design with auxetic I and it was about 100.7 times for numerical simulation and 77.3 times in experimental measurements.

CRediT authorship contribution statement

Conceptualization, **D.Y.** and **A.H.**; Methodology, **D.Y., A.H.** and **F.E.**; Software **A.H.** and **F.E.**; Formal analysis, **A.H.** and **F.E.**; Resources, **A.M.**; Data curation, **A.H., F.E.** and **A.M.**; Writing – original draft, **A.H.** and **D.Y.**; Writing – review & editing, **D.Y.**; Visualization, **A.H.** and **F.E.**.

Submission declaration and verification

This paper has not been published previous and is not under consideration for publication elsewhere.

Declaration of Competing Interest

The authors declare that they have no known competing financial interests or personal relationships that could have appeared to influence the work reported in this paper.

Acknowledgement

There is no governmental or external fund to support this study.

References

[1] H. Askari, E. Hashemi, A. Khajepour, M.B. Khamesee, Z.L. Wang, Towards self-powered sensing using nanogenerators for automotive systems, Nano Energy 53 (2018) 1003–1019, https://doi.org/10.1016/j.nanoen.2018.09.032.
[2] A. Hosseinkhani, D. Younesian, P. Eghbali, A. Moayedizadeh, A. Fassih, Sound and vibration energy harvesting for railway applications: a review on linear and nonlinear techniques, Energy Rep. 7 (2021) 852–874, https://doi.org/10.1016/J.EGYR.2021.01.087.
[3] M. Yuan, Z. Cao, J. Luo, X. Chou, Recent developments of acoustic energy harvesting: a review, Micromachines 10 (2019) 48, https://doi.org/10.3390/mi10010048.
[4] H. Askari, A. Khajepour, M.B. Khamesee, Z.L. Wang, Embedded self-powered sensing systems for smart vehicles and intelligent transportation, Nano Energy 66 (2019), 104103, https://doi.org/10.1016/J.NANOEN.2019.104103.
[5] G. Jing, M. Siahkouhi, J. Riley Edwards, M.S. Dersch, N.A. Hoult, Smart railway sleepers - a review of recent developments, challenges, and future prospects, Constr. Build. Mater. (2020), 121533, https://doi.org/10.1016/j.conbuildmat.2020.121533.
[6] Z.L. Wang, Nanogenerators, self-powered systems, blue energy, piezotronics and piezo-phototronics – a recall on the original thoughts for coining these fields, Nano Energy 54 (2018) 477–483, https://doi.org/10.1016/j.nanoen.2018.09.068.
[7] F.K. Shaikh, S. Zeadally, Energy harvesting in wireless sensor networks: a comprehensive review, Renew. Sustain. Energy Rev. 55 (2016) 1041–1054, https://doi.org/10.1016/j.rser.2015.11.010.
[8] O. Jo, Y.K. Kim, J. Kim, Internet of things for smart railway: feasibility and applications, IEEE Internet Things J. 5 (2018) 482–490.
[9] S.P. Beeby, M.J. Tudor, N.M. White, Energy harvesting vibration sources for microsystems applications, Meas. Sci. Technol. 17 (2006) R175, https://doi.org/10.1088/0957-0233/17/12/R01.
[10] C. Wei, X. Jing, A comprehensive review on vibration energy harvesting: modelling and realization, Renew. Sustain. Energy Rev. 74 (2017) 1–18, https://doi.org/10.1016/j.rser.2017.01.073.
[11] S. Shahab, S. Leadenham, F. Guillot, K. Sabra, A. Erturk, Ultrasound acoustic wave energy transfer and harvesting, Act. Passiv. Smart Struct. Integr. Syst. 9057 (2014) 90570F, https://doi.org/10.1117/12.2045198.
[12] T. Li, P.S. Lee, Piezoelectric energy harvesting with an ultrasonic vibration source, Actuators 8 (2019) 8, https://doi.org/10.3390/ACT8010008.
[13] C.R. Farrar, G. Park, T. Rosing, M.D. Todd, W. Hodgkiss, Energy harvesting for structural health monitoring sensor networks, J. Infrastruct. Syst. 14 (2008) 64–79, https://doi.org/10.1061/(ASCE)1076-0342(2008)14:1(64).
[14] D. Younesian, M.-R. Alam, Multi-stable mechanisms for high-efficiency and broadband ocean wave energy harvesting, Appl. Energy 197 (2017) 292–302, https://doi.org/10.1016/J.APENERGY.2017.04.019.
[15] W.J.G. Ferguson, Y. Kuang, K.E. Evans, C.W. Smith, M. Zhu, Auxetic structure for increased power output of strain vibration energy harvester, Sens. Actuators A Phys. 282 (2018) 90–96, https://doi.org/10.1016/J.SNA.2018.09.019.
[16] Z. Chen, B. Guo, Y. Yang, C. Cheng, Metamaterials-based enhanced energy harvesting: a review, Phys. B Condens. Matter 438 (2014) 1–8, https://doi.org/10.1016/J.PHYSB.2013.12.040.
[17] S.H. Jo, H. Yoon, Y.C. Shin, B.D. Youn, A graded phononic crystal with decoupled double defects for broadband energy localization, Int. J. Mech. Sci. 183 (2020), 105833, https://doi.org/10.1016/j.ijmecsci.2020.105833.
[18] F. Ebrahimian, Z. Kabirian, D. Younesian, P. Eghbali, Auxetic clamped-clamped resonators for high-efficiency vibration energy harvesting at low-frequency excitation, Appl. Energy 295 (2021), 117010, https://doi.org/10.1016/J.APENERGY.2021.117010.
[19] T.G. Lee, S.H. Jo, H.M. Seung, S.W. Kim, E.J. Kim, B.D. Youn, S. Nahm, M. Kim, Enhanced energy transfer and conversion for high performance phononic crystal-assisted elastic wave energy harvesting, Nano Energy 78 (2020), 105226, https://doi.org/10.1016/J.NANOEN.2020.105226.
[20] T. Li, Z. Wang, H. Xiao, Z. Yan, C. Yang, T. Tan, Dual-band piezoelectric acoustic energy harvesting by structural and local resonances of Helmholtz metamaterial, Nano Energy 90 (2021), 106523, https://doi.org/10.1016/J.NANOEN.2021.106523.
[21] A. Moayedizadeh, D. Younesian, Application of the meta-substrates for power amplification in rotary piezoelectric energy harvesting systems: design, fabrication and testing, Energy Rep. 8 (2022) 5653–5667, https://doi.org/10.1016/j.egyr.2022.04.022.
[22] X. Yu, J. Zhou, H. Liang, Z. Jiang, L. Wu, Mechanical metamaterials associated with stiffness, rigidity and compressibility: a brief review, Prog. Mater. Sci. 94 (2018) 114–173, https://doi.org/10.1016/J.PMATSCI.2017.12.003.
[23] M.H. Lu, L. Feng, Y.F. Chen, Phononic crystals and acoustic metamaterials, Mater. Today 12 (2009) 34–42, https://doi.org/10.1016/S1369-7021(09)70315-3.
[24] P. Martakis, G. Aguzzi, V.K. Dertimanis, E.N. Chatzi, A. Colombi, Nonlinear periodic foundations for seismic protection: practical design, realistic evaluation and stability considerations, Soil Dyn. Earthq. Eng. 150 (2021), 106934, https://doi.org/10.1016/J.SOILDYN.2021.106934.
[25] B. Florijn, C. Coulais, M. van Hecke, Programmable mechanical metamaterials: the role of geometry, Soft Matter 12 (2016) 8736–8743, https://doi.org/10.1039/C6SM01271J.
[26] M. Miniaci, A. Krushynska, A.S. Gliozzi, N. Kherraz, F. Bosia, N.M. Pugno, Design and fabrication of bioinspired hierarchical dissipative elastic metamaterials, Phys. Rev. Appl. 10 (2018), 024012, https://doi.org/10.1103/PhysRevApplied.10.024012.
[27] J. Xiong, L. Ma, L. Wu, B. Wang, A. Vaziri, Fabrication and crushing behavior of low density carbon fiber composite pyramidal truss structures, Compos. Struct. 92 (2010) 2695–2702, https://doi.org/10.1016/J.COMPSTRUCT.2010.03.010.
[28] M.S. Mazloomi, M. Ranjbar, L. Boldrin, F. Scarpa, S. Patsias, N. Ozada, Vibroacoustics of 2D gradient auxetic hexagonal honeycomb sandwich panels, Compos. Struct. 187 (2018) 593–603, https://doi.org/10.1016/j.compstruct.2017.10.077.
[29] L. D'Alessandro, V. Zega, R. Ardito, A. Corigliano, 3D auxetic single material periodic structure with ultra-wide tunable bandgap, Sci. Rep. 8 (2018) 2262, https://doi.org/10.1038/s41598-018-19963-1.
[30] Y. Umino, T. Tsukamoto, S. Shiomi, K. Yamada, T. Suzuki, Development of vibration energy harvester with 2D mechanical metamaterial structure, J. Phys. Conf. Ser. 1052 (2018), 012103, https://doi.org/10.1088/1742-6596/1052/1/012103.
[31] N. Chandrasekharan, L.L. Thompson, Increased power to weight ratio of piezoelectric energy harvesters through integration of cellular honeycomb structures, Smart Mater. Struct. 25 (2016), 045019, https://doi.org/10.1088/0964-1726/25/4/045019.
[32] Z. Kabirian, F. Ebrahimian, D. Younesian, P. Eghbali, Inlay-inspired meta-piezoelectric plates for the low-frequency vibration energy harvesting, J. Mater. Sci. Mater. Electron. 33 (2022) 2909–2920, https://doi.org/10.1007/S10854-021-07489-8.
[33] M.L. De Bellis, A. Bacigalupo, Auxetic behavior and acoustic properties of microstructured piezoelectric strain sensors, Smart Mater. Struct. 26 (2017), 085037, https://doi.org/10.1088/1361-665X/AA7772.
[34] P. Eghbali, D. Younesian, A. Moayedizadeh, M. Ranjbar, Study in circular auxetic structures for efficiency enhancement in piezoelectric vibration energy harvesting, Sci. Rep. 10 (2020) 1–11.
[35] Q. Li, Y. Kuang, M. Zhu, Auxetic piezoelectric energy harvesters for increased electric power output, AIP Adv. 7 (2017), 015104, https://doi.org/10.1063/1.4974310.
[36] P. Eghbali, D. Younesian, S. Farhangdoust, Enhancement of the low-frequency acoustic energy harvesting with auxetic resonators, Appl. Energy 270 (2020), 115217, https://doi.org/10.1016/j.apenergy.2020.115217.

[37] S.L. Zhang, Y.-C. Lai, X. He, R. Liu, Y. Zi, Z.L. Wang, Auxetic foam-based contact-mode triboelectric nanogenerator with highly sensitive self-powered strain sensing capabilities to monitor human body movement, Adv. Funct. Mater. 27 (2017), 1606695, https://doi.org/10.1002/ADFM.201606695.
[38] P.A. Deymier, Acoustic Metamaterials and Phononic Crystals, Springer Science & Business Media, 2013, https://doi.org/10.1007/978-3-642-31232-8.
[39] C. Croënne, E.J.S. Lee, H. Hu, J.H. Page, Band gaps in phononic crystals: generation mechanisms and interaction effects, AIP Adv. 1 (2011), 041401, https://doi.org/10.1063/1.3675797.
[40] K.C. Chuang, Z.W. Yuan, Y.Q. Guo, X.F. Lv, Extracting torsional band gaps and transient waves in phononic crystal beams: method and validation, J. Sound Vib. 467 (2020), 115004, https://doi.org/10.1016/j.jsv.2019.115004.
[41] J. Vondřejc, E. Rohan, J. Heczko, Shape optimization of phononic band gap structures using the homogenization approach, Int. J. Solids Struct. 113–114 (2017) 147–168, https://doi.org/10.1016/J.IJSOLSTR.2017.01.038.
[42] E. Panahi, A. Hosseinkhani, M.F. Khansanami, D. Younesian, M. Ranjbar, Novel cross shape phononic crystals with broadband vibration wave attenuation characteristic: design, modeling and testing, Thin Walled Struct. 163 (2021), 107665, https://doi.org/10.1016/J.TWS.2021.107665.
[43] A.O. Krushynska, V.G. Kouznetsova, M.G.D. Geers, Towards optimal design of locally resonant acoustic metamaterials, J. Mech. Phys. Solids 71 (2014) 179–196, https://doi.org/10.1016/j.jmps.2014.07.004.
[44] A. Hosseinkhani, D. Younesian, M. Ranjbar, F. Scarpa, Enhancement of the vibro-acoustic performance of anti-tetra-chiral auxetic sandwich panels using topologically optimized local resonators, Appl. Acoust. 177 (2021), 107930.
[45] M. Sigalas, E.N. Economou, Band structure of elastic waves in two dimensional systems, Solid State Commun. 86 (1993) 141–143.
[46] S. Wen, Y. Xiong, S. Hao, F. Li, C. Zhang, Enhanced band-gap properties of an acoustic metamaterial beam with periodically variable cross-sections, Int. J. Mech. Sci. 166 (2020), 105229, https://doi.org/10.1016/j.ijmecsci.2019.105229.
[47] G.J. Chaplain, J.M. De Ponti, G. Aguzzi, A. Colombi, R.V. Craster, Topological rainbow trapping for elastic energy harvesting in graded Su-Schrieffer-Heeger systems, Phys. Rev. Appl. 14 (2020), 054035, https://doi.org/10.1103/PhysRevApplied.14.054035.
[48] P. Wang, J. Shim, K. Bertoldi, Effects of geometric and material nonlinearities on tunable band gaps and low-frequency directionality of phononic crystals, Phys. Rev. B. 88 (2013), 014304, https://doi.org/10.1103/PhysRevB.88.014304.
[49] S. Timorian, M. Ouisse, N. Bouhaddi, S. De Rosa, F. Franco, Numerical investigations and experimental measurements on the structural dynamic behaviour of quasi-periodic meta-materials, Mech. Syst. Signal Process. 136 (2020), 106516, https://doi.org/10.1016/j.ymssp.2019.106516.
[50] S.-Y. Chang, C.-D. Chen, J.-Y. Yeh, L.-W. Chen, Elastic wave propagation of two-dimensional metamaterials composed of auxetic star-shaped honeycomb structures, Crystals 9 (2019) 121, https://doi.org/10.3390/cryst9030121.
[51] A.O. Krushynska, N. Anerao, M.A. Badillo-Ávila, M. Stokroos, M. Acuautla, Arbitrary-curved waveguiding and broadband attenuation in additively manufactured lattice phononic media, Mater. Des. 205 (2021), 109714, https://doi.org/10.1016/j.matdes.2021.109714.
[52] L.Y. Wu, L.W. Chen, C.M. Liu, Experimental investigation of the acoustic pressure in cavity of a two-dimensional sonic crystal, Phys. B Condens. Matter 404 (2009) 1766–1770, https://doi.org/10.1016/J.PHYSB.2009.02.025.
[53] C.S. Park, Y.C. Shin, S.H. Jo, H. Yoon, W. Choi, B.D. Youn, M. Kim, Two-dimensional octagonal phononic crystals for highly dense piezoelectric energy harvesting, Nano Energy 57 (2019) 327–337, https://doi.org/10.1016/J.NANOEN.2018.12.026.
[54] Y. Li, T. Chen, X. Wang, T. Ma, P. Jiang, Acoustic confinement and waveguiding in two-dimensional phononic crystals with material defect states, J. Appl. Phys. 116 (2014), 024904, https://doi.org/10.1063/1.4889846.
[55] S. Tol, F.L. Degertekin, A. Erturk, Gradient-index phononic crystal lens-based enhancement of elastic wave energy harvesting, Appl. Phys. Lett. 109 (2016), 063902, https://doi.org/10.1063/1.4960792.
[56] S. Tol, F.L. Degertekin, A. Erturk, Phononic crystal Luneburg lens for omnidirectional elastic wave focusing and energy harvesting, Appl. Phys. Lett. 111 (2017), 013503, https://doi.org/10.1063/1.4991684.
[57] L.-Y. Wu, L.-W. Chen, C.-M. Liu, Acoustic energy harvesting using resonant cavity of a sonic crystal, Appl. Phys. Lett. 95 (2009), 013506, https://doi.org/10.1063/1.3176019.
[58] H. Lv, X. Tian, M.Y. Wang, D. Li, Vibration energy harvesting using a phononic crystal with point defect states, Appl. Phys. Lett. 102 (2013), 034103, https://doi.org/10.1063/1.4788810.
[59] Z.Q. Lu, L. Zhao, H. Ding, L.Q. Chen, A dual-functional metamaterial for integrated vibration isolation and energy harvesting, J. Sound Vib. 509 (2021), 116251, https://doi.org/10.1016/J.JSV.2021.116251.
[60] K. Mikoshiba, J.M. Manimala, C.T. Sun, Energy harvesting using an array of multifunctional resonators, J. Intell. Mater. Syst. Struct. 24 (2012) 168–179, https://doi.org/10.1177/1045389X12460335.
[61] L.Y. Wu, M.L. Wu, L.W. Chen, The narrow pass band filter of tunable 1D phononic crystals with a dielectric elastomerlayer, Smart Mater. Struct. 18 (2008), 015011, https://doi.org/10.1088/0964-1726/18/1/015011.
[62] Y.Z. Wang, F.M. Li, Y.S. Wang, Influences of active control on elastic wave propagation in a weakly nonlinear phononic crystal with a monoatomic lattice chain, Int. J. Mech. Sci. 106 (2016) 357–362, https://doi.org/10.1016/J.IJMECSCI.2015.12.004.
[63] Y.W. Zhang, C. Su, Z.Y. Ni, J. Zang, L.Q. Chen, A multifunctional lattice sandwich structure with energy harvesting and nonlinear vibration control, Compos. Struct. 221 (2019), 110875, https://doi.org/10.1016/J.COMPSTRUCT.2019.04.047.
[64] P.U. Kelkar, H.S. Kim, K.H. Cho, J.Y. Kwak, C.Y. Kang, H.C. Song, Cellular auxetic structures for mechanical metamaterials: a review, Sensors 20 (2020) 3132, https://doi.org/10.3390/s20113132.
[65] M. Safaei, H.A. Sodano, S.R. Anton, A review of energy harvesting using piezoelectric materials: state-of-the-art a decade later (2008–2018), Smart Mater. Struct. 28 (2019), 113001, https://doi.org/10.1088/1361-665X/AB36E4.
[66] W. Ku, T. Berlijn, C.-C. Lee, Unfolding first-principles band structures, Phys. Rev. Lett. 104 (2010), 216401, https://doi.org/10.1103/PhysRevLett.104.216401.
[67] L.Y. Wu, L.W. Chen, Propagation of acoustic waves in the woodpile sonic crystal with a defect, Appl. Acoust. 73 (2012) 312–322, https://doi.org/10.1016/J.APACOUST.2011.10.002.
[68] F. Wu, Z. Liu, Y. Liu, Splitting and tuning characteristics of the point defect modes in two-dimensional phononic crystals, Phys. Rev. E 69 (2004), 066609, https://doi.org/10.1103/PhysRevE.69.066609.
[69] S.H. Jo, H. Yoon, Y.C. Shin, W. Choi, C.S. Park, M. Kim, B.D. Youn, Designing a phononic crystal with a defect for energy localization and harvesting: supercell size and defect location, Int. J. Mech. Sci. 179 (2020), 105670, https://doi.org/10.1016/j.ijmecsci.2020.105670.

Ali Hosseinkhani received his B.Sc. degree from Sirjan University of Technology, Sirjan, Iran, in 2014 and M.Sc. and Ph.D. from Iran University of Science and Technology, Tehran, Iran in 2017 and 2022, in Mechanical Engineering. He attended as a Ph.D. visiting student at Politecnico di Milano, Milan, Italy from 2020 to 2021. Ali is currently a Sessional Instructor at Iran University of Science and Technology.

Fariba Ebrahimian received the B.Sc. degree from Isfahan University, Isfahan, Iran in 2019 and M.Sc. degree from Iran University of Science and Technology, Tehran, Iran in 2021, all in Mechanical Engineering (Major in Rolling stock). Her research interests include metamaterials and vibration energy harvesting.

Davood Younesian received Ph.D. degree in Mechanical Engineering from Sharif University of Technology, Iran in 2004. He attended two post-doctoral fellowships in nonlinear/random vibration of flexible structures at ISVR, University of Southampton, UK and at University of Ontario Institute of Technology, Canada 2004–2006. He also attended University of California at Berkeley in 2016 as visiting scholar for one year. He has already published more than 150 journal papers and 4 books in the area of vibration, control and acoustics. He is now full professor and serving as vice-chancellor for research and technology at Iran University of Science and Technology.

Armin Moayedizadeh is currently a Ph.D. candidate in Mechanical Engineering at Iran University of Science and Technology (IUST). He received his B.Sc. in Mechanical Engineering from Amirkabir University of Technology, Tehran, Iran in 2014 and his M.Sc. in Mechanical Engineering from IUST, Tehran, Iran, in 2017. His research interest includes FEM modeling and experimental characterization of piezoelectric meta-material energy harvesting systems.